NANO LETTERS

pubs.acs.org/NanoLett Letter

Reconfigurable Magnetic Liquid Metal Robot for High-Performance Droplet Manipulation

Yuxuan Zhang, Shaojun Jiang, Yanlei Hu,* Tao Wu, Yiyuan Zhang, Huizeng Li, An Li, Yachao Zhang, Hao Wu, Yinlong Ding, Erqiang Li, Jiawen Li, Dong Wu,* Yanlin Song, and Jiaru Chu

Cite This: *Nano Lett.* 2022, 22, 2923–2933 Read Online

ACCESS | Metrics & More | Article Recommendations | Supporting Information

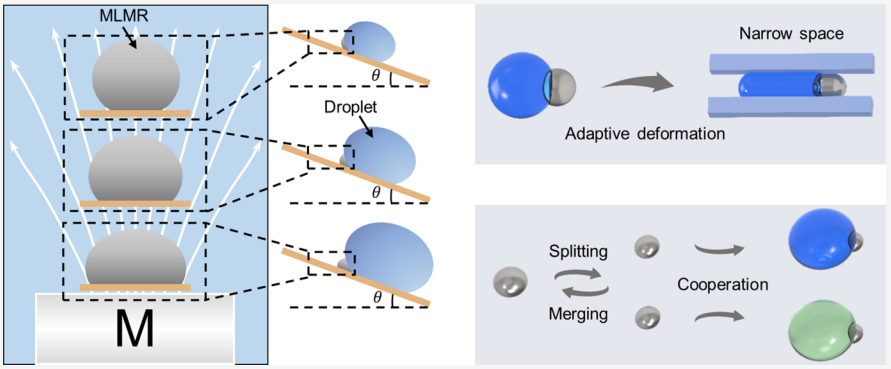

ABSTRACT: Droplet manipulation is crucial for diverse applications ranging from bioassay to medical diagnosis. Current magnetic-field-driven manipulation strategies are mainly based on fixed or partially tunable structures, which limits their flexibility and versatility. Here, a reconfigurable magnetic liquid metal robot (MLMR) is proposed to address these challenges. Diverse droplet manipulation behaviors including steady transport, oscillatory transport, and release can be achieved by the MLMR, and their underlying physical mechanisms are revealed. Moreover, benefiting from the magnetic-field-induced active deformability and temperature-induced phase transition characteristics, its droplet-loading capacity and shape-locking/unlocking switching can be flexibly adjusted. Because of the fluidity-based adaptive deformability, MLMR can manipulate droplets in challenging confined environments. Significantly, MLMR can accomplish cooperative manipulation of multiple droplets efficiently through on-demand self-splitting and merging. The high-performance droplet manipulation using the reconfigurable and multifunctional MLMR unfolds new potential in microfluidics, biochemistry, and other interdisciplinary fields.

KEYWORDS: *magnetic liquid metal robot, droplet manipulation, high-performance, multifunctional, active and passive deformability, splitting capability*

1. INTRODUCTION

Controllable droplet manipulation, such as capture, transport, merging, and mixing of droplets, plays a crucial role in various fields including chemical and biological analysis,[1−3] medical detection,[4,5] and biosensing.[6] In order to achieve the efficient droplet manipulation, diverse external stimuli have been explored including surface acoustic wave,[7] light,[8,9] magnetic field,[10,11] electric field,[12−15] and mechanical vibration.[16,17] Because of the advantages of noncontact, biocompatibility, and real-time control,[18] the use of magnetic fields to manipulate droplets has attracted broad attention in recent years. Magnetic-actuated droplet manipulation can be roughly divided into two categories. In the first category, various magnetoresponsive structures are developed for the droplet manipulation.[19−21] However, the manufacturing and modification process is quite complicated, and the flexibility of droplet manipulation is restricted by predesigned structures. In addition, it is difficult to achieve the desired droplet manipulation in constrained workspace. In the second category, droplets are combined with magnetic particles or beads to move under an external magnetic field.[22−24] For example, a magnetically actuated robot consisting of two steel beads was proposed to achieve programmable droplet manipulation. Nevertheless, the transport speed and droplet volume are limited. Because of the rigid robot structure, it cannot be applied in some confined environments, such as narrow channels much smaller than its size.[23] Therefore, how to devise an intelligent strategy to realize

Received: January 10, 2022
Revised: March 17, 2022
Published: March 25, 2022

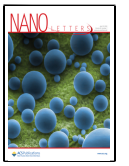

https://doi.org/10.1021/acs.nanolett.2c00100
Nano Lett. 2022, 22, 2923−2933

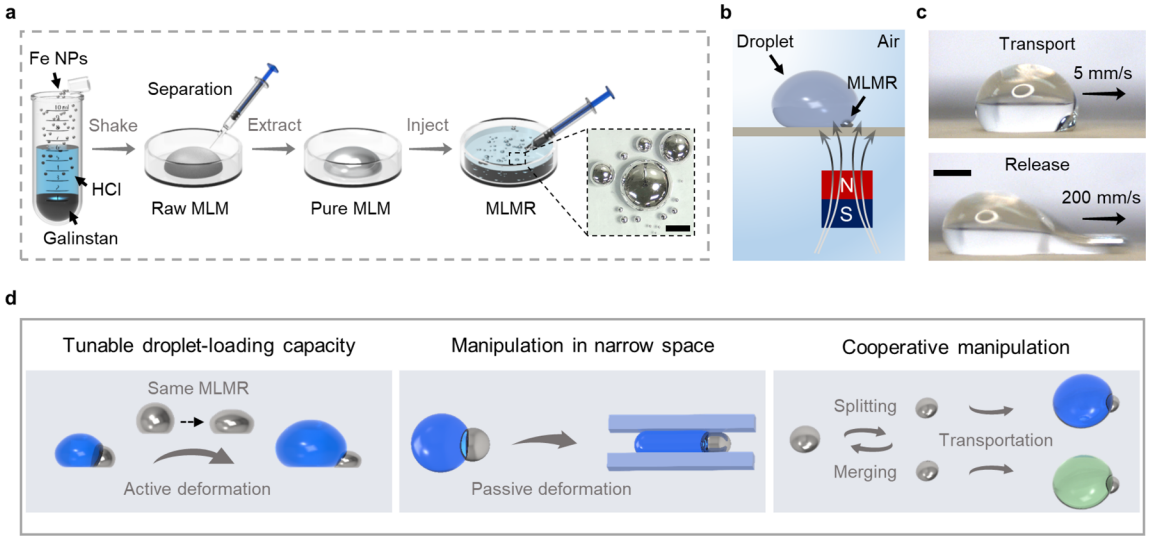

Figure 1. Preparation of MLMR and its reconfigurable characteristics in droplet manipulation. (a) Preparation of MLMR. The inset image shows the generated MLMRs with different diameters. They range in size from micrometers to millimeters. (b) Schematics of the droplet manipulation system. (c) Optical images of the droplet transport and release. The droplet volume is ~50 μL. When the speed of MLMR (diameter of ~1.25 mm) is 5 mm/s, the liquid−gas interface can restrain the MLMR, and the TCL can provide the adhesion force to drive the droplet. While the speed of MLMR is 200 mm/s, the interface fails to restrain the MLMR, resulting in the release of the droplet. The magnetic flux density (B) on the surface is ~100 mT. (d) Illustration of the unique droplet manipulation capabilities of MLMR. The prepared MLMR has reconfigurable characteristics and can be used to realize unique droplet manipulation. When exposed to a stronger magnetic field, the same MLMR can transport a larger droplet through its active deformation. The MLMR has great passive deformability and can adapt to constrained environments to complete challenging droplet manipulations in narrow space. It can be split into smaller sub-MLMRs or remerge on demand to manipulate multiple droplets for cooperative manipulation missions. Scale bars: 5 mm in (a) and 2 mm in (c).

high-performance droplet manipulation with great flexibility and versatility is still a challenge.

Gallium-based liquid metals (LMs), such as gallium (Ga), eutectic gallium−indium alloys (EGaIn), and gallium−indium-tin alloys (Galinstan), are attractive and promising because of the combination of unique fluidic and metallic properties (high surface tension, high electrical/thermal conductivity, high fluidity, and low toxicity).[25,26] These characteristics make them especially favorable in diverse applications including soft robots,[27,28] stretchable and wearable electronics,[29,30] and microelectromechanical actuators.[31] Furthermore, LMs can be mixed with magnetic particles to acquire magnetic response property.[32,33] Although LMs can be used in diverse fields, their applications in droplet manipulation remain to be explored.

Herein, a reconfigurable magnetic liquid metal robot (MLMR) is developed to achieve high-performance and multifunctional droplet manipulation. By taking advantage of hydrophilicity and instantaneous magnetic responsiveness, the MLMR can drive the droplet under external magnetic field, which does not require additional complex structures. The different droplet manipulation behaviors of MLMR including steady transport, oscillatory transport, and release are modeled and analyzed systematically. Besides, flexible and programmable droplet transportation with large volume range (5−1100 μL) and speed range (1−180 mm/s) can be realized. The three-dimensional (3D) droplet capture-transport-release process is showcased. Particularly, the droplet transport capacity can be flexibly modulated in situ by adjusting the magnetic-field-induced active deformation of MLMR. Furthermore, benefiting from the low melting point and exceptional photothermal properties, MLMR possesses the shape-locking and shape-unlocking capabilities induced by phase transition under natural cooling and near-infrared (NIR) irradiation. Because of the excellent fluidity-based passive deformability of MLMR, droplet manipulation in confined space can be achieved, which is challenging for other manipulation methods. More interestingly, a single MLMR can be split into several sub-MLMRs under the critical magnetic field, which can be used to cooperatively manipulate multiple droplets. Multifunctional applications including stimuli-free antigravity droplet pinning, droplet collection in challenging confined space, active droplet mixing, efficient chemical reaction, and magnetically controlled droplet circuit switch are demonstrated. Our proposed reconfigurable MLMR can achieve high-performance, flexible, and versatile droplet manipulation, which shows great potential in the fields of microfluidics, biomedical devices, and chemistry.

2. RESULTS AND DISCUSSION

2.1. Preparation of MLMR and its Reconfigurable Characteristics in Droplet Manipulation. The preparation process of MLMR is schematically illustrated in Figure 1a. Hydrochloric acid solution (HCl, 2 M), Galinstan, and iron nanoparticles (Fe NPs, diameter of ~100 nm) are successively added into the container. The HCl solution can eliminate the oxides and make Fe NPs more conductive and polarizable than Galinstan, allowing the particles to be suspended into Galinstan.[34] Then, the container is sealed and shaken sufficiently to facilitate the suspension. A galvanic cell can be formed between Fe NPs and Ga of Galinstan, which oxidizes Ga while protecting Fe NPs from the chemical reaction with HCl (Figure S1). When the mixture solution becomes transparent from being turbid, it indicates that Fe NPs have been successfully suspended into Galinstan. The relatively pure magnetic liquid metal (MLM) wrapped in the oxide film is then extracted for further use, which looks shiny (see Figure S2 for snapshots and SEM images). When injected into the sodium hydroxide (NaOH) solution, the MLM can break into small droplets due to the high surface tension and fluids interaction. By changing the injection

https://doi.org/10.1021/acs.nanolett.2c00100
Nano Lett. 2022, 22, 2923−2933

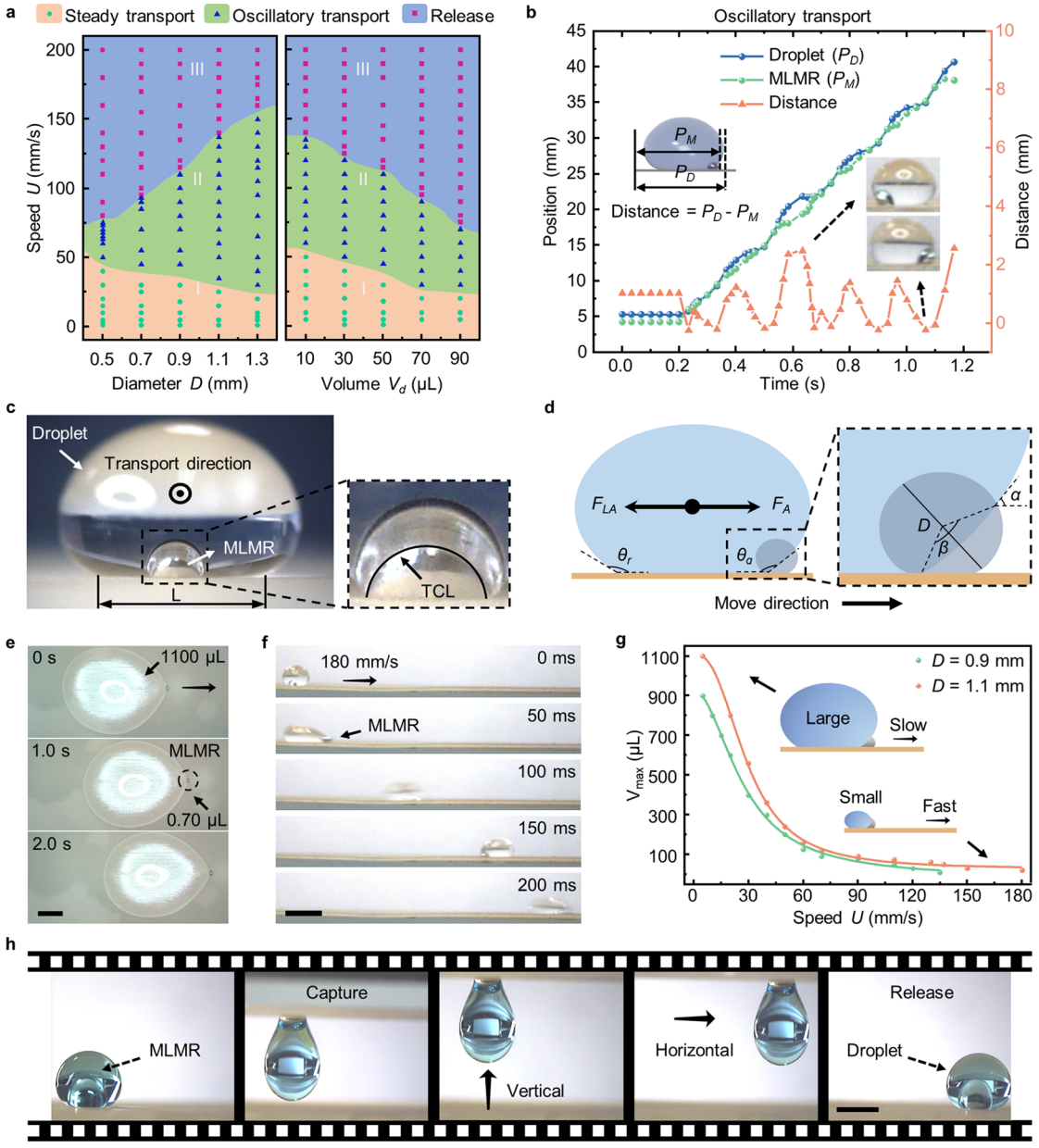

Figure 2. Analysis and demonstration of high-performance droplet manipulation. (a) Phase diagrams demonstrating the diverse droplet manipulation modes with variation of the diameter of MLMR (D), droplet volume (V_d), and speed of MLMR (U). In the left phase diagram, V_d = 50 μL. In the right phase diagram, D = 0.9 mm. (b) The positions of droplet and MLMR and their relative distance versus time under the oscillatory transport mode. The droplet (~20 μL) is transported by the MLMR (D = 1.1 mm) at 30 mm/s. When calculating the positions of the droplet and MLMR (P_D and P_M), the reference line is selected as the leftmost end of the substrate in the captured image. The distance is defined as P_D minus P_M, that is, distance = $P_D - P_M$. The two inset optical images show the relative positions of the droplet and MLMR at different moments. (c) Optical image showing the TCL during steady transport. The droplet (~50 μL) is transported steadily by the MLMR (D = 1.1 mm) at 5 mm/s under B = 145 mT. The moving direction is perpendicular to the plane outward. (d) Modeling and mechanical analysis to explain the different droplet manipulation behaviors of MLMR. (e) Transport of a huge droplet. The droplet (~1100 μL) is transported by the MLMR (D = 1.1 mm, volume of ~0.70 μL) at 5 mm/s. (f) High-speed transport of a droplet. The droplet (~20 μL) is transported at 180 mm/s (oscillatory transport mode) by the MLMR (D = 1.1 mm). (g) Dependence of the maximum volume of transportable droplet (V_{max}) on the speed of MLMR (U). The diameters of MLMRs in the two experimental groups are ~0.9 and ~1.1 mm, respectively. The dots denote the experimental results. The lines indicate the nonlinear fitting curves. (h) Efficient 3D droplet manipulation. MLMR can realize the capture, vertical transport, horizontal transport, and release of the droplet at any position flexibly. When the droplet dyed blue (~15 μL) is captured and held by the MLMR (D = 1.3 mm), B is ~150 mT on the upper surface. In (a,b,e,f,g), $B \approx$ 100 mT. Scale bars: 5 mm in (e,f) and 2 mm in (h).

velocity and syringe aperture size, the MLMRs with different diameters (from micrometer to millimeter scale) can be generated (Movie S1).[35]

Droplet transport and release are two primary functions in our droplet manipulation system composed of an MLMR, a permanent magnet, and a superhydrophobic substrate (Figure 1b). Femtosecond laser ablation is used to construct hierarchical micro/nanoscale structures on polydimethylsiloxane (PDMS) films to fabricate the superhydrophobic substrates (Figure S3).[36] The effect of different laser scanning speeds on

https://doi.org/10.1021/acs.nanolett.2c00100
Nano Lett. 2022, 22, 2923−2933

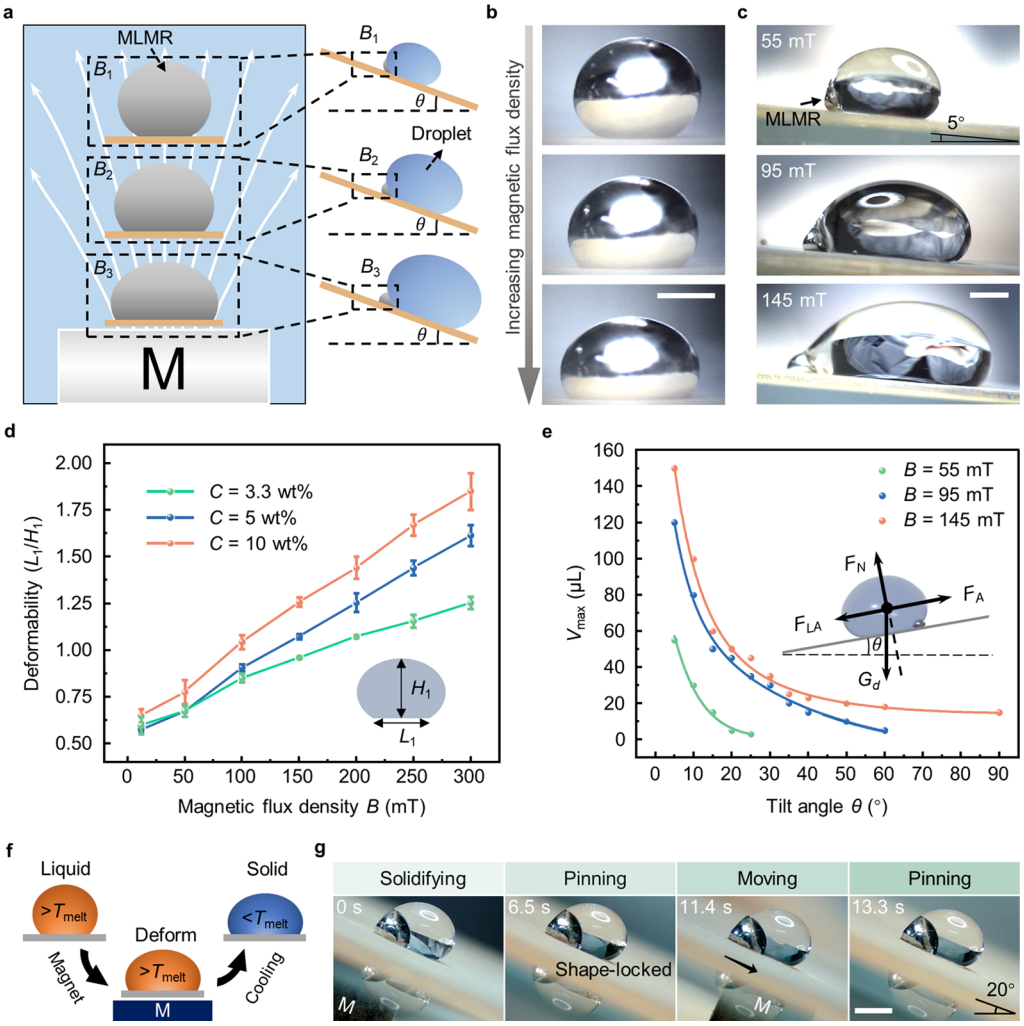

Figure 3. Active control of MLMR by magnetic and thermal fields. (a) Schematic illustration of the adjustable droplet transport capacity of MLMR enabled by its active deformability. (b) Magnetically responsive active deformation. The MLMR (D = 2.6 mm) is subjected to different magnetic fields ($B \approx$ 50, 150, 250 mT) and its active deformations are recorded. (c) Demonstration of the adjustable droplet transport capacity. The maximum volumes of transportable droplets (V_{max}) of the MLMR (D = 1.3 mm) under different B (55, 95, 145 mT) on the inclined surface (tilt angle θ of ~5°) are 55, 120, and 150 μL, respectively. (d) Dependence of the active deformability on Fe NPs concentration (C) and magnetic flux density. The active deformability (L_1/H_1) of MLMR (D = 2.6 mm) with different C (3.3 wt %, 5 wt %, 10 wt %) under different B is calculated. (e) Effect of magnetic flux density and tilt angle on the droplet transport capacity. V_{max} of the MLMR (D = 1.3 mm) on the inclined surfaces with different θ under different B (55, 95, 145 mT) are recorded. The inset shows the mechanical model. (f) Schematics of the temperature-induced shape-locking capability. When $T > T_{melt}$, the MLMR is liquid and can be deformed by the magnetic field. After sufficient cooling ($T < T_{melt}$), it becomes solid and its deformation can be locked. (g) Shape-locking-based antigravity droplet pinning. The liquid MLMR (D = 1.9 mm) deforms under the magnetic field and locks its deformation after sufficient natural cooling. The shape-locked MLMR can pin the droplet (~15 μL) on the inclined plane (θ = 20°) even if the droplet is transported to other positions. The action line of the resultant force of the driving forces on the solidified MLMR is within its friction angle (self-locking effect). This antigravity droplet pinning based on shape locking does not require any external energy input. Scale bars: 1 mm in (b) and 2 mm in (c,g).

superhydrophobicity is studied (Figure S4). The magnet is placed below the substrate and the dependence of magnetic flux density (B) on distance is investigated (Figure S5). By virtue of the great magnetic responsiveness and inherent hydrophilicity, MLMR can move with the magnet and adhere to the droplet to provide a driving force for desired manipulation, including droplet capture, transport, and release (Figure 1c, Figure S6, and Movie S2). The different droplet motion modes are mainly determined by the competitive relationship between surface tension and inertial force. Particularly, when the external magnetic field is properly applied, MLMR can exhibit reconfigurable characteristics and further enables unique droplet manipulation capabilities,[37,38] including in situ tunable droplet-loading capacity through its magnetic-field-induced active deformation, flexible droplet manipulation in challenging narrow space through its fluidity-based passive deformation, and cooperative droplet manipulation through its controllable self-splitting/merging behaviors (Figure 1d).

2.2. Analysis and Demonstration of High-performance Droplet Manipulation. In order to demonstrate the droplet manipulation capability of MLMR, the influence of the diameter (D) and velocity (U) of MLMR and droplet volume (V_d) on horizontal droplet manipulation modes is systematically investigated (Figure 2a). The manipulation behaviors of MLMR can be divided into three modes, namely steady transport, oscillatory transport, and release. To investigate the differences

https://doi.org/10.1021/acs.nanolett.2c00100
Nano Lett. 2022, 22, 2923−2933

between these modes intuitively, the positions and relative distances of the droplet (V_d = 20 μL) and MLMR (D = 1.1 mm) during three typical manipulations are recorded, respectively (Figure S7 and Figure 2b). When the MLMR starts to move at a low speed (region I), there is a stable three-phase contact line (TCL) between the droplet and MLMR (Figure 2c and Movie S3)[39] and thereby the steady transport can be achieved (see Figure S8 for speed relationship). When the MLMR starts to move at a moderate speed (region II), the inertial force of MLMR is not enough to overcome the constraint of droplet surface tension. However, the MLMR brings great initial deformation to the droplet. In this case, the droplet behaves like a mass-spring system and oscillates during its movement (Figure 2b).[40] When the speed of MLMR is high enough (region III), it can break through the liquid−gas interface and release the droplet (see Figures S9−S11 for snapshots of these three typical manipulation processes).[41,42]

To explain the different modes caused by the interaction between the droplet, MLMR, and substrate, a mechanical model is developed (Figure 2d). First, the capillary number Ca, a ratio of viscous force to surface tension, is about 10^{-3}, indicating that viscosity is ignorable compared to surface tension.[43] Therefore, only two forces are considered: the driving force is the adhesion force (F_A) exerted on the droplet by the TCL between the droplet and MLMR,[23] while the resisting force is the lateral adhesion force (F_{LA}) between the droplet and substrate.[44] They can be expressed respectively as[23,44,45]

$$F_A \sim \gamma \pi D \sin\frac{\beta}{2}\cos\alpha \tag{1}$$

$$F_{LA} \sim k\gamma L(\cos\theta_r - \cos\theta_a) \tag{2}$$

where γ, β, α, k, L, θ_r, and θ_a are the droplet surface tension, position angle of the TCL, angle between the tangent line of the TCL and move direction, dimensionless factor,[44] droplet contact width (Figure 2c), receding contact angle, and advancing contact angle, respectively. Then, we figure out the critical conditions between the different modes. The critical velocity between the transport mode and release mode (U_{tr}, region I + II and region III) and the critical velocity between the steady transport mode and oscillatory transport mode (U_{so}, region I and region II) of MLMR can be expressed, respectively, as follows (see Note S1 in Supporting Information for detailed analysis)[45]

$$U_{tr} \sim \frac{\pi D\gamma^{5/4}\sin\frac{\beta}{2}\cos\alpha}{\rho_d^{5/4}V_d g_m^{3/4}} \sim \frac{D}{V_d} \tag{3}$$

$$U_{so} \sim \frac{1}{\sqrt{DV_d}} \tag{4}$$

where ρ_d and g_m are the droplet density and the acceleration of MLMR, respectively. From eqs 3 and 4, it can be seen that U_{tr} is proportional to D and inversely proportional to V_d, while U_{so} is negatively correlated with D and V_d, which is almost consistent with the experimental results in Figure 2a.

Because of the strong adhesion to droplet, MLMR can achieve the droplet transport in a large volume range and speed range. As shown in Figure 2e, the huge droplet (~1100 μL) can be transported by the tiny MLMR (volume ratio of droplet to MLMR ~1571). Figure 2f shows that the droplet can be transported at a very high speed (~180 mm/s). The maximum volume of transportable droplets (V_{max}) of MLMR at different speeds is investigated (Figure 2g). It can be seen that V_{max} decreases with the increase of U, and a larger MLMR can transport a larger droplet at the same speed. Moreover, the droplet motion can be flexibly and programmably controlled, as demonstrated in Figures S12−S14.[46] Interestingly, MLMR can even realize the 3D droplet manipulation (Figure S15, Figure 2h, Movie S4). The largest droplet that can be manipulated by MLMR with different diameters in this 3D mode is investigated in Figure S16 (see Note S2 in Supporting Information for mechanical analysis). Furthermore, the MLMR can manipulate droplets on other untreated surfaces (Figures S17−S19).

2.3. Active Control of MLMR by Magnetic and Thermal Fields. It is noteworthy that the shape and liquid/solid state of MLMR can be intelligently controlled by external magnetic and thermal fields. The shape of a sessile liquid MLMR is mainly determined by the interplay between surface tension, gravity, and magnetic forces.[47] As the magnetic flux density (B) increases, the shape of MLMR gradually changes from approximately spherical to flat, and the maximum adhesion force it can provide for manipulating droplet also increases (see Note S3 in Supporting Information for detailed analysis). Therefore, the maximum volume of transportable droplets (V_{max}) on the same inclined plane increases with the increase of B (Figure 3a−c). To study the influence of Fe NPs concentration (C) and B on the active deformability of MLMR, the MLMRs with different C (3.3 wt %, 5 wt %, 10 wt %) are prepared (see Figure S20 for the effect of C on magnetic response performance). We record the deformation and calculate the ratio of contact width L_1 to height H_1 of the deformed MLMR (L_1/H_1, defined as the deformability), while varying B (Figure 3d, see Figure S21 and Movie S5 for more demonstrations). Then, the scaling analysis is carried out to model the active deformability of MLMR. The dimensionless forms of L_1 and H_1 can be expressed as $L_1/(D/2) \sim (DMB/2\sigma)^{1/4}$ and $H_1/(D/2) \sim (DMB/2\sigma)^{-1/2}$ respectively,[48] where M is the magnetization of MLMR given by $M = B\chi/[\mu_0(1+\chi)]$ (χ, μ_0, and σ are the magnetic susceptibility of MLMR, magnetic permeability of free space, and surface tension of MLMR, respectively).[49] Therefore, we can obtain

$$\frac{L_1}{H_1} \sim \left(\frac{DMB}{2\sigma}\right)^{3/4} \tag{5}$$

With the increase of B and C (C is positively correlated with M), L_1/H_1 increases, which shows great consistency with Figure 3d. To prove the active-deformation-based adjustable droplet-loading capacity of MLMR, V_{max} on the inclined plane with different tilt angles (θ) under different B is investigated (Figure 3e). It can be seen that V_{max} decreases with the increase of θ and increases with B (see Note S4 in Supporting Information for detailed analysis). For example, when B is ~95 mT, V_{max} of the MLMR with a diameter of ~1.3 mm on the inclined plane with θ = 5° is ~120 μL (Movie S6). Importantly, this magnetic-field-induced active deformability of MLMR enables its in situ tunable droplet transport capacity, which is appealing for on-demand droplet manipulation.

In addition, because of the low melting point and outstanding photothermal properties of MLMR,[50,51] it can realize phase transition between solid and liquid under natural cooling and NIR irradiation. Thus, the friction characteristics between the MLMR and substrate can be tuned, which contributes to the desired motion control of droplets. When the temperature of MLMR (T) is above its melting point ($T > T_{melt}$), the MLMR is

https://doi.org/10.1021/acs.nanolett.2c00100
Nano Lett. 2022, 22, 2923−2933

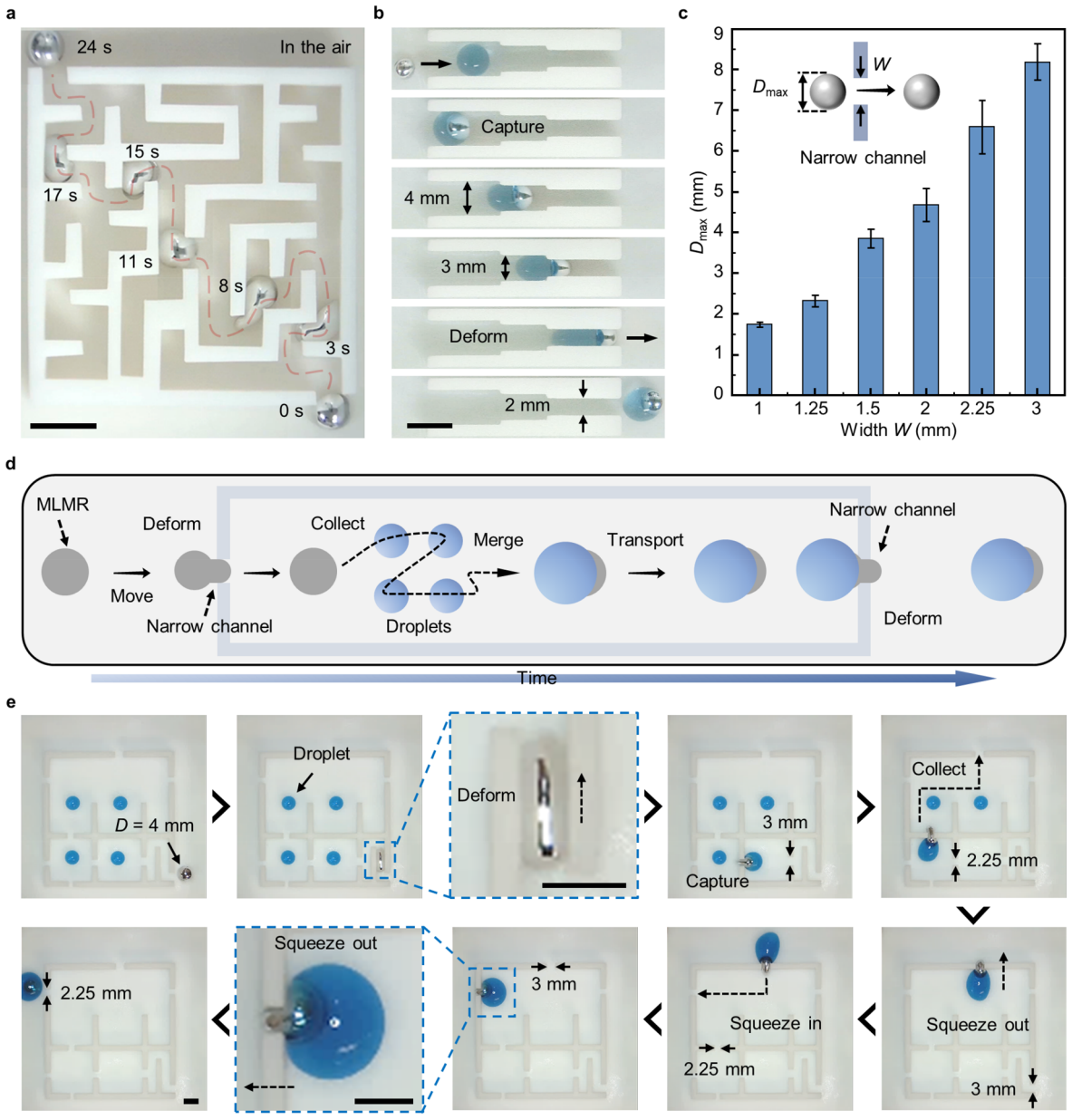

Figure 4. Passive deformability of MLMR based on fluidity. (a) Navigation of the MLMR through various narrow channels in a maze. The MLMR (D = 5 mm) passes through a series of narrow channels freely through adaptive deformation. The sequential snapshots are overlapped in one image for clear display. (b) Droplet transport in confined space. The MLMR (D = 2.3 mm) can capture and carry the droplet (~20 μL) through the narrow channels flexibly. (c) Relationship between the maximum diameter of MLMR (D_{max}) and the width of narrow channel (W). The MLMRs with different diameters are driven to pass through the narrow channel (W = 1, 1.25, 1.5, 2, 2.25, 3 mm) at 15 mm/s. The inset shows the schematic. The maximum diameters of MLMR allowed to pass through these narrow channels are recorded, respectively. (d) Schematics and (e) video snapshots of the droplet collection in confined space. Four droplets dyed blue (volume of each ~50 μL) at different positions in the confined structure are captured, collected, and transported sequentially by the MLMR (D = 4 mm) through the narrow channels with different widths (minimum width ~2.25 mm). B is ~100 mT on the surface. The surfaces of these experimental structures are all superhydrophobized using commercial superhydrophobic coatings. Scale bars: 10 mm in (a) and 5 mm in (b,e).

liquid and can be deformed by the magnetic field. After being cooled to $T < T_{melt}$, it solidifies and its active deformation can be locked (Figure 3f, Figure S22).[50] The shape-locked solid MLMR can be driven to move but cannot be deformed by magnetic field, while its shape can be unlocked by sufficient NIR irradiation (Figure S23). As demonstrated in Figure S24, two connected solid MLMRs can melt and merge with each other under NIR light. On the basis of the shape-locking capability of MLMR, the stimuli-free antigravity droplet pinning is demonstrated (Figure 3g). The liquid MLMR is placed on the inclined plane ($\theta = 20°$) and the magnetic field is applied. After natural cooling, the solidified MLMR locks its active deformation and enables the droplet pinning at any position without a magnetic field (Movie S7). The friction-based self-locking effect between the solid MLMR and inclined substrate,[52] as well as the strong adhesion between the MLMR and droplet, is conducive to the successful stimuli-free antigravity droplet pinning.

2.4. Passive Deformability of MLMR based on Fluidity.

Apart from the active deformability and phase-transition capability, MLMR also possesses the fluidity-based passive

https://doi.org/10.1021/acs.nanolett.2c00100
Nano Lett. 2022, 22, 2923−2933

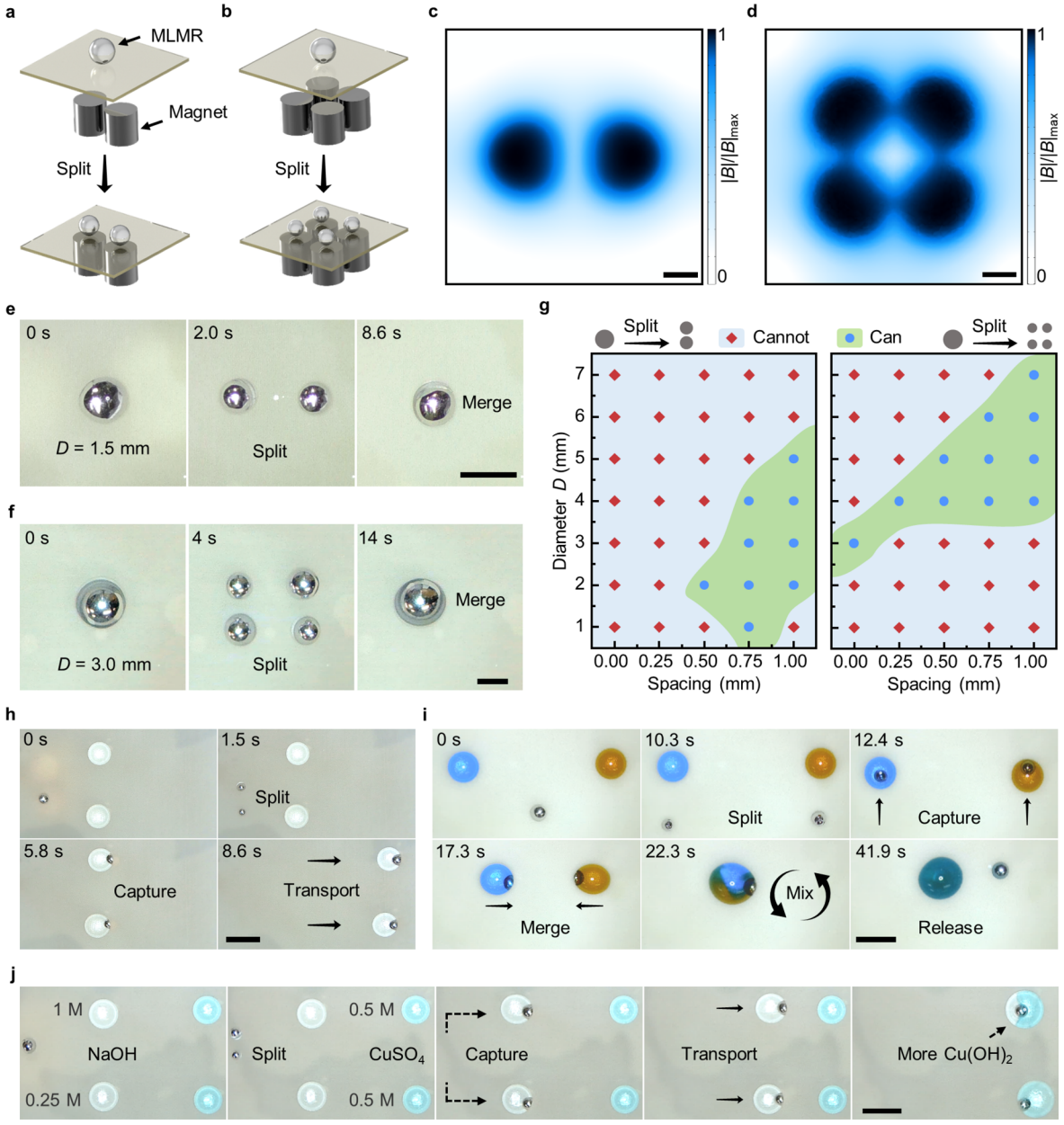

Figure 5. Splitting capability of MLMR induced by magnetic field. (a,b) Schematics of the magnetic-field-induced splitting. The schematics show that one MLMR can be split into (a) two or (b) four sub-MLMRs. (c,d) Distributions of the critical magnetic fields on the substrate surface. The two magnetic fields are generated by (c) two magnets with spacing of ~0.75 mm and (d) four magnets with spacing of ~0 mm, respectively. The distance between the magnets (Φ5 mm × 5 mm) and surface is ~0.8 mm. (e,f) Snapshots of the splitting and merging process. When exposed to the magnetic fields in (c,d), the MLMR can be split into two and four sub-MLMRs, respectively. These sub-MLMRs can be reversibly merged. (g) Phase diagrams demonstrating the splitting capability, when varying the diameter of MLMR and magnet spacing. The left and right phase diagrams show whether the MLMR can be split into two and four sub-MLMRs, respectively. (h) Demonstration of the efficient droplet transport. The MLMR (D = 1.4 mm) is split into two sub-MLMRs, which can be used to transport two different droplets (~20 μL). (i) Snapshots of the efficient droplet mixing process. Two droplets dyed in different colors (blue and orange, ~30 μL) are transported, merged, and mixed efficiently through on-demand splitting and merging behaviors of the MLMR (D = 1.9 mm). Finally, the uniformly mixed droplet is released. (j) Demonstration of the efficient chemical reaction. Two NaOH droplets with different concentrations (~20 μL, 1 and 0.25 M) are driven separately by two daughter MLMRs obtained from the splitting of the mother MLMR (D = 1.5 mm) to react with the $CuSO_4$ droplets (~20 μL, 0.5 M). The $Cu(OH)_2$ precipitates are formed immediately. More precipitates in the upper merged droplet indicate that the NaOH concentration is higher before the reaction. The spacing between the two magnets for splitting the MLMR is ~0.75 mm in (h,j), while ~0.5 mm in (i). Scale bars: 2 mm in (c–f) and 5 mm in (h–j).

deformability where its shape can adapt to the confined environments. This adaptive deformability enables MLMR to realize droplet manipulation in challenging narrow space, which is difficult for other reported manipulation methods. In Figure 4a, we demonstrate that MLMR can navigate in a complex maze with various narrow channels (see Figure S25 for preparation process and SEM image of the superhydrophobic 3D-printed structure). During the navigation, the MLMR can change its shape to adapt to the meandering narrow channels easily. More importantly, it is demonstrated that MLMR can capture and carry a droplet through narrow channels (Figure 4b). To understand the passive deformability of MLMR, the maximum

https://doi.org/10.1021/acs.nanolett.2c00100
Nano Lett. 2022, 22, 2923−2933

diameter of MLMRs (D_{max}) that can be allowed to pass through the narrow channels of different widths (W) is investigated (Figure 4c, see Figure S26 for optical images). For example, the MLMR with diameter of ~6.88 mm can squeeze through a narrow channel (W = 2.25 mm) about three times smaller than its own size. Since MLMR has extraordinary adaptive deformability and noncontact controllability, it can realize droplet collection and transportation in difficult-to-access confined environments (Figure 4d,e). During the collection, the droplets can be carried through the extremely narrow channels freely (Movie S8), manifesting the applicability of MLMR in challenging constrained space.

2.5. Splitting Capability of MLMR induced by Magnetic Field. Interestingly, when subjected to the critical confining magnetic field from two or four cylindrical permanent magnets aligned with the same polarity, a single MLMR can be split into two or four small sub-MLMRs respectively (Figure 5a,b). The magnetic-field-induced splitting capability of MLMR results from the combination of high magnetic field and high magnetic field gradient,[47] which depends on the appropriate interaction between magnetic force and surface tension.[53] When the MLMR is exposed to a magnetic field, the exerted horizontal magnetic force can be expressed as[49,54,55]

$$F_m \sim \frac{B(\nabla B)\chi\pi D^3}{6\mu_0(1+\chi)} \quad (6)$$

where ∇B is the gradient of B. Therefore, magnetic fields with special distributions can exert magnetic forces on MLMR in different directions, contributing to the splitting behaviors of MLMR.[55] For example, when two cylindrical magnets (Φ5 mm × 5 mm, spacing of ~0.75 mm, spacing is defined as the shortest distance between the edges of two adjacent magnets, Figure S27) approach slowly until the distance between the magnets and substrate reaches the critical value (~0.8 mm, see Figure 5c for the 2D critical magnetic field distribution), the MLMR can be split into two sub-MLMRs (Figure 5e). During the splitting process, the MLMR is subjected to two opposite magnetic pulling forces (Figure S28). Similarly, when exposed to the critical magnetic field generated by four magnets with spacing of ~0 mm (Figure 5d), the MLMR can be divided into four sub-MLMRs (Figure 5f). By controlling the magnetic field, the sub-MLMRs can be merged reversibly. The splitting behaviors of MLMR mainly depend on its size and the distribution of applied magnetic field.[47,53] Figure 5g shows whether the MLMR can be split into two or four sub-MLMRs when both varying its diameter and the spacing of two or four magnets, respectively (see Figures S29−S31 for more demonstrations).

More significantly, the magnetic-field-induced splitting and merging capabilities of MLMR provide the possibility for collaborative droplet manipulation.[24] Figure 5h demonstrates that two sub-MLMRs can simultaneously capture and transport two droplets. The rapid merging and uniform mixing of droplets are essential for practical applications such as biochemical analysis and substance detection.[20,24] For demonstration, the efficient droplet mixing is performed by using the on-demand splitting and merging abilities of MLMR (Figure 5i). Furthermore, the splitting capability of MLMR can also be utilized for chemical reaction (Figure 5j).[56] The NaOH droplets (~20 μL) of different concentrations (1 M, 0.25 M) are individually captured and transported by the obtained two sub-MLMRs. Then, they are separately merged and reacted with two copper sulfate droplets (~20 μL, $CuSO_4$) of the same concentration (0.5 M). The amount of formed copper hydroxide ($Cu(OH)_2$) precipitates can reflect the concentration difference of the two NaOH droplets (Movie S9). Therefore, the chemical reaction and concentration detection can be realized simultaneously. In addition, the MLMR and droplet can be integrated as a magnetically controlled droplet circuit switch (Figure S32), which can be used to connect and disconnect the electronic circuit reversibly (Movie S10).

3. CONCLUSION

In summary, a reconfigurable MLMR with great flexibility and versatility is proposed for high-performance droplet manipulation. Different manipulation modes including steady transport, oscillatory transport, and release can be realized, and the underlying physical mechanisms are systematically investigated. Moreover, MLMR enables the large-volume (~1100 μL) and high-speed (~180 mm/s) droplet transport and efficient 3D droplet manipulation. By controlling the strength of applied magnetic field, the droplet transport capacity of MLMR can be flexibly adjusted in situ owing to its active deformability. Remarkably, due to the low melting point and high photothermal conversion efficiency, MLMR can realize phase-transition-based shape locking/unlocking under natural cooling and NIR irradiation. Benefiting from the exceptional fluidity-based passive deformability, MLMR can carry a droplet through narrow channels much smaller than its size in confined environments. Furthermore, the magnetic-field-induced splitting and merging capabilities of MLMR are also revealed, which can be utilized to complete cooperative manipulation of different droplets. Multiple functionalities of MLMR, including stimuli-free antigravity droplet pinning, adaptive-deformation-based droplet collection in narrow space, active droplet mixing, efficient chemical reaction, and magnetically controlled droplet-driving-based circuit switching, are explored. The proposed droplet manipulation strategy using the reconfigurable MLMR has promising prospects in biochemical analysis, microfluidics, and interdisciplinary fields.

■ ASSOCIATED CONTENT

Supporting Information

The Supporting Information is available free of charge at https://pubs.acs.org/doi/10.1021/acs.nanolett.2c00100.

Generation of MLMRs with different diameters (MP4)
Transport and release of droplet (MP4)
Three-phase contact line in steady transport (MP4)
Demonstration of high-performance droplet manipulation (MP4)
Active deformability of MLMR (MP4)
Transport of droplet on the inclined surface (MP4)
Demonstration of phase-transition-based shape-locking/unlocking capability (MP4)
Demonstration of passive deformability (MP4)
Demonstration of splitting capability (MP4)
Magnetically controlled droplet circuit switch (MP4)
Experimental section, equations, SEM, figures, optical images, detailed mechanical analysis (PDF)

■ AUTHOR INFORMATION

Corresponding Authors

Yanlei Hu − *CAS Key Laboratory of Mechanical Behavior and Design of Materials, Key Laboratory of Precision Scientific Instrumentation of Anhui Higher Education Institutes,*

https://doi.org/10.1021/acs.nanolett.2c00100
Nano Lett. 2022, 22, 2923−2933

Department of Precision Machinery and Precision Instrumentation, University of Science and Technology of China, Hefei 230027, China; orcid.org/0000-0003-1964-0043; Email: huyl@ustc.edu.cn

Dong Wu − *CAS Key Laboratory of Mechanical Behavior and Design of Materials, Key Laboratory of Precision Scientific Instrumentation of Anhui Higher Education Institutes, Department of Precision Machinery and Precision Instrumentation, University of Science and Technology of China, Hefei 230027, China;* orcid.org/0000-0003-0623-1515; Email: dongwu@ustc.edu.cn

Authors

Yuxuan Zhang − *CAS Key Laboratory of Mechanical Behavior and Design of Materials, Key Laboratory of Precision Scientific Instrumentation of Anhui Higher Education Institutes, Department of Precision Machinery and Precision Instrumentation, University of Science and Technology of China, Hefei 230027, China;* orcid.org/0000-0003-1699-9894

Shaojun Jiang − *CAS Key Laboratory of Mechanical Behavior and Design of Materials, Key Laboratory of Precision Scientific Instrumentation of Anhui Higher Education Institutes, Department of Precision Machinery and Precision Instrumentation, University of Science and Technology of China, Hefei 230027, China*

Tao Wu − *Department of Modern Mechanics, University of Science and Technology of China, Hefei 230027, China;* orcid.org/0000-0002-0291-6595

Yiyuan Zhang − *CAS Key Laboratory of Mechanical Behavior and Design of Materials, Key Laboratory of Precision Scientific Instrumentation of Anhui Higher Education Institutes, Department of Precision Machinery and Precision Instrumentation, University of Science and Technology of China, Hefei 230027, China;* orcid.org/0000-0002-0393-2597

Huizeng Li − *Key Laboratory of Green Printing, Institute of Chemistry, Chinese Academy of Sciences, Beijing 100190, China;* orcid.org/0000-0001-6689-6637

An Li − *Key Laboratory of Green Printing, Institute of Chemistry, Chinese Academy of Sciences, Beijing 100190, China*

Yachao Zhang − *CAS Key Laboratory of Mechanical Behavior and Design of Materials, Key Laboratory of Precision Scientific Instrumentation of Anhui Higher Education Institutes, Department of Precision Machinery and Precision Instrumentation, University of Science and Technology of China, Hefei 230027, China*

Hao Wu − *CAS Key Laboratory of Mechanical Behavior and Design of Materials, Key Laboratory of Precision Scientific Instrumentation of Anhui Higher Education Institutes, Department of Precision Machinery and Precision Instrumentation, University of Science and Technology of China, Hefei 230027, China*

Yinlong Ding − *CAS Key Laboratory of Mechanical Behavior and Design of Materials, Key Laboratory of Precision Scientific Instrumentation of Anhui Higher Education Institutes, Department of Precision Machinery and Precision Instrumentation, University of Science and Technology of China, Hefei 230027, China*

Erqiang Li − *Department of Modern Mechanics, University of Science and Technology of China, Hefei 230027, China*

Jiawen Li − *CAS Key Laboratory of Mechanical Behavior and Design of Materials, Key Laboratory of Precision Scientific Instrumentation of Anhui Higher Education Institutes, Department of Precision Machinery and Precision Instrumentation, University of Science and Technology of China, Hefei 230027, China;* orcid.org/0000-0003-3950-6212

Yanlin Song − *Key Laboratory of Green Printing, Institute of Chemistry, Chinese Academy of Sciences, Beijing 100190, China;* orcid.org/0000-0002-0267-3917

Jiaru Chu − *CAS Key Laboratory of Mechanical Behavior and Design of Materials, Key Laboratory of Precision Scientific Instrumentation of Anhui Higher Education Institutes, Department of Precision Machinery and Precision Instrumentation, University of Science and Technology of China, Hefei 230027, China;* orcid.org/0000-0001-6472-8103

Complete contact information is available at: https://pubs.acs.org/10.1021/acs.nanolett.2c00100

Author Contributions

Y.Z. (Yuxuan Zhang), Y.H., and D.W. designed the project. Y.Z. (Yuxuan Zhang) performed the experiments. S.J., Y.H., Y.Z. (Yiyuan Zhang), H.L., A.L., Y.Z. (Yachao Zhang), H.W., Y.D., D.W., and Y.S. provided constructive suggestions. Y.Z. (Yuxuan Zhang), T.W., and E.L. developed the theoretical model and analyzed the data. Y.Z. (Yuxuan Zhang), S.J., and Y.H. wrote the paper with input from all other authors. J.L., D.W., Y.S., and J.C. supervised the research. All authors made comments and approved the manuscript.

Notes

The authors declare no competing financial interest.

■ ACKNOWLEDGMENTS

This work was supported by the National Natural Science Foundation of China (Nos. 61927814, 52122511, 91963127, 51875544, 52105492, U20A20290), Major Scientific and Technological Projects in Anhui Province (201903a05020005), and the Fundamental Research Funds for the Central Universities (YD2090002005, WK2090000024). We acknowledge the Experimental Center of Engineering and Material Sciences at USTC for the fabrication and measuring of samples. This work was partly carried out at the USTC Center for Micro and Nanoscale Research and Fabrication.

■ REFERENCES

(1) Tang, X.; Zhu, P.; Tian, Y.; Zhou, X.; Kong, T.; Wang, L. Mechano-regulated surface for manipulating liquid droplets. *Nat. Commun.* **2017**, *8*, 14831.

(2) Bawazer, L. A.; McNally, C. S.; Empson, C. J.; Marchant, W. J.; Comyn, T. P.; Niu, X.; Cho, S.; McPherson, M. J.; Binks, B. P.; deMello, A.; Meldrum, F. C. Combinatorial microfluidic droplet engineering for biomimetic material synthesis. *Sci. Adv.* **2016**, *2*, e1600567.

(3) Lee, B.; Jin, S. H.; Noh, Y.; Jeong, S.; Jeong, H.; Lee, C. Scalable static droplet array for biochemical assays based on concentration gradients. *Sens. Actuators, B* **2018**, *273*, 1572−1578.

(4) Serra, M.; Ferraro, D.; Pereiro, I.; Viovy, J. L.; Descroix, S. The power of solid supports in multiphase and droplet-based microfluidics: towards clinical applications. *Lab Chip* **2017**, *17*, 3979−3999.

(5) Hajji, I.; Serra, M.; Geremie, L.; Ferrante, I.; Renault, R.; Viovy, J. L.; Descroix, S.; Ferraro, D. Droplet microfluidic platform for fast and continuous-flow RT-qPCR analysis devoted to cancer diagnosis application. *Sens. Actuators, B* **2020**, *303*, 127171.

(6) Chen, Y.; Li, K.; Zhang, S.; Qin, L.; Deng, S.; Ge, L.; Xu, L. P.; Ma, L.; Wang, S.; Zhang, X. Bioinspired Superwettable Microspine Chips with Directional Droplet Transportation for Biosensing. *ACS Nano* **2020**, *14*, 4654−4661.
(7) Shilton, R. J.; Travagliati, M.; Beltram, F.; Cecchini, M. Nanoliter-droplet acoustic streaming via ultra high frequency surface acoustic waves. *Adv. Mater.* **2014**, *26*, 4941−4946.
(8) Lv, J. A.; Liu, Y.; Wei, J.; Chen, E.; Qin, L.; Yu, Y. Photocontrol of fluid slugs in liquid crystal polymer microactuators. *Nature* **2016**, *537*, 179−184.
(9) Kwon, G.; Panchanathan, D.; Mahmoudi, S. R.; Gondal, M. A.; McKinley, G. H.; Varanasi, K. K. Visible light guided manipulation of liquid wettability on photoresponsive surfaces. *Nat. Commun.* **2017**, *8*, 14968.
(10) Dorvee, J. R.; Derfus, A. M.; Bhatia, S. N.; Sailor, M. J. Manipulation of liquid droplets using amphiphilic, magnetic one-dimensional photonic crystal chaperones. *Nat. Mater.* **2004**, *3*, 896−899.
(11) Si, Y.; Hu, J.; Dong, Z. Bioinspired magnetically driven liquid manipulation as microrobot. *Cell Rep. Phys. Sci.* **2021**, *2*, 100439.
(12) Li, J.; Ha, N. S.; Liu, T. L.; van Dam, R. M.; Kim, C.-J. Ionic-surfactant-mediated electro-dewetting for digital microfluidics. *Nature* **2019**, *572*, 507−510.
(13) Zhang, Y.; Wittstock, G. A Platform for Electric Field Aided and Wire-Guided Droplet Manipulation. *Small* **2017**, *13*, 1601691.
(14) Sun, Q.; Wang, D.; Li, Y.; Zhang, J.; Ye, S.; Cui, J.; Chen, L.; Wang, Z.; Butt, H. J.; Vollmer, D.; Deng, X. Surface charge printing for programmed droplet transport. *Nat. Mater.* **2019**, *18*, 936−941.
(15) Jin, Y.; Xu, W.; Zhang, H.; Li, R.; Sun, J.; Yang, S.; Liu, M.; Mao, H.; Wang, Z. Electrostatic tweezer for droplet manipulation. *Proc. Natl. Acad. Sci. U. S. A.* **2022**, *119*, e2105459119.
(16) Brunet, P.; Eggers, J.; Deegan, R. D. Vibration-induced climbing of drops. *Phys. Rev. Lett.* **2007**, *99*, 144501.
(17) Wu, D.; Zhang, Z.; Zhang, Y.; Jiao, Y.; Jiang, S.; Wu, H.; Li, C.; Zhang, C.; Li, J.; Hu, Y.; Li, G.; Chu, J.; Jiang, L. High-Performance Unidirectional Manipulation of Microdroplets by Horizontal Vibration on Femtosecond Laser-Induced Slant Microwall Arrays. *Adv. Mater.* **2020**, *32*, 2005039.
(18) Zhou, Y.; Huang, S.; Tian, X. Magnetoresponsive Surfaces for Manipulation of Nonmagnetic Liquids: Design and Applications. *Adv. Funct. Mater.* **2020**, *30*, 1906507.
(19) Zhang, Y.; Huang, Z.; Cai, Z.; Ye, Y.; Li, Z.; Qin, F.; Xiao, J.; Zhang, D.; Guo, Q.; Song, Y.; Yang, J. Magnetic-actuated "capillary container" for versatile three-dimensional fluid interface manipulation. *Sci. Adv.* **2021**, *7*, eabi7498.
(20) Jiang, S.; Hu, Y.; Wu, H.; Li, R.; Zhang, Y.; Chen, C.; Xue, C.; Xu, B.; Zhu, W.; Li, J.; Wu, D.; Chu, J. Three-Dimensional Multifunctional Magnetically Responsive Liquid Manipulator Fabricated by Femtosecond Laser Writing and Soft Transfer. *Nano Lett.* **2020**, *20*, 7519−7529.
(21) Lei, W.; Hou, G.; Liu, M.; Rong, Q.; Xu, Y.; Tian, Y.; Jiang, L. High-speed transport of liquid droplets in magnetic tubular micro-actuators. *Sci. Adv.* **2018**, *4*, eaau8767.
(22) Zhang, Y.; Wang, T. H. Full-range magnetic manipulation of droplets via surface energy traps enables complex bioassays. *Adv. Mater.* **2013**, *25*, 2903−2908.
(23) Li, A.; Li, H.; Li, Z.; Zhao, Z.; Li, K.; Li, M.; Song, Y. Programmable droplet manipulation by a magnetic-actuated robot. *Sci. Adv.* **2020**, *6*, eaay5808.
(24) Yu, W. Z.; Lin, H. S.; Wang, Y. L.; He, X.; Chen, N.; Sun, K.; Lo, D.; Cheng, B.; Yeung, C.; Tan, J. W.; Di Carlo, D.; Emaminejad, S. A ferrobotic system for automated microfluidic logistics. *Sci. Robot.* **2020**, *5*, eaba4411.
(25) Yun, G.; Tang, S. Y.; Sun, S.; Yuan, D.; Zhao, Q.; Deng, L.; Yan, S.; Du, H.; Dickey, M. D.; Li, W. Liquid metal-filled magnetorheological elastomer with positive piezoconductivity. *Nat. Commun.* **2019**, *10*, 1300.
(26) Chen, S.; Wang, H.; Zhao, R.; Rao, W.; Liu, J. Liquid Metal Composites. *Matter* **2020**, *2*, 1446−1480.
(27) Ford, M. J.; Ambulo, C. P.; Kent, T. A.; Markvicka, E. J.; Pan, C.; Malen, J.; Ware, T. H.; Majidi, C. A multifunctional shape-morphing elastomer with liquid metal inclusions. *Proc. Natl. Acad. Sci. U. S. A.* **2019**, *116*, 21438−21444.
(28) Wang, X.; Guo, R.; Liu, J. Liquid Metal Based Soft Robotics: Materials, Designs, and Applications. *Adv. Mater. Technol.* **2019**, *4*, 1800549.
(29) Markvicka, E. J.; Bartlett, M. D.; Huang, X.; Majidi, C. An autonomously electrically self-healing liquid metal-elastomer composite for robust soft-matter robotics and electronics. *Nat. Mater.* **2018**, *17*, 618−624.
(30) Dickey, M. D. Stretchable and Soft Electronics using Liquid Metals. *Adv. Mater.* **2017**, *29*, 1606425.
(31) Tang, S. Y.; Khoshmanesh, K.; Sivan, V.; Petersen, P.; O'Mullane, A. P.; Abbott, D.; Mitchell, A.; Kalantar-zadeh, K. Liquid metal enabled pump. *Proc. Natl. Acad. Sci. U. S. A.* **2014**, *111*, 3304−3309.
(32) Cao, L.; Yu, D.; Xia, Z.; Wan, H.; Liu, C.; Yin, T.; He, Z. Ferromagnetic Liquid Metal Putty-Like Material with Transformed Shape and Reconfigurable Polarity. *Adv. Mater.* **2020**, *32*, 2000827.
(33) Ma, B.; Xu, C.; Chi, J.; Chen, J.; Zhao, C.; Liu, H. A Versatile Approach for Direct Patterning of Liquid Metal Using Magnetic Field. *Adv. Funct. Mater.* **2019**, *29*, 1901370.
(34) Carle, F.; Bai, K.; Casara, J.; Vanderlick, K.; Brown, E. Development of magnetic liquid metal suspensions for magneto-hydrodynamics. *Phys. Rev. Fluids* **2017**, *2*, 013301.
(35) Yu, Y.; Wang, Q.; Yi, L. T.; Liu, J. Channelless Fabrication for Large-Scale Preparation of Room Temperature Liquid Metal Droplets. *Adv. Eng. Mater.* **2014**, *16*, 255−262.
(36) Yong, J.; Chen, F.; Li, M.; Yang, Q.; Fang, Y.; Huo, J.; Hou, X. Remarkably simple achievement of superhydrophobicity, superhydrophilicity, underwater superoleophobicity, underwater superoleophilicity, underwater superaerophobicity, and underwater superaerophilicity on femtosecond laser ablated PDMS surfaces. *J. Mater. Chem. A* **2017**, *5*, 25249−25257.
(37) Liu, X.; Kent, N.; Ceballos, A.; Streubel, R.; Jiang, Y.; Chai, Y.; Kim, P. Y.; Forth, J.; Hellman, F.; Shi, S.; Wang, D.; Helms, B. A.; Ashby, P. D.; Fischer, P.; Russell, T. P. Reconfigurable ferromagnetic liquid droplets. *Science* **2019**, *365*, 264−267.
(38) Wu, X.; Streubel, R.; Liu, X.; Kim, P. Y.; Chai, Y.; Hu, Q.; Wang, D.; Fischer, P.; Russell, T. P. Ferromagnetic liquid droplets with adjustable magnetic properties. *Proc. Natl. Acad. Sci. U. S. A.* **2021**, *118*, e2017355118.
(39) Eggers, J. Hydrodynamic theory of forced dewetting. *Phys. Rev. Lett.* **2004**, *93*, 094502.
(40) Han, X.; Li, W.; Zhao, H.; Li, J.; Tang, X.; Wang, L. Slippery damper of an overlay for arresting and manipulating droplets on nonwetting surfaces. *Nat. Commun.* **2021**, *12*, 3154.
(41) Takamure, K.; Uchiyama, T. Air−water interface dynamics and energy transition in air of a sphere passed vertically upward through the interface. *Exp. Therm Fluid Sci.* **2020**, *118*, 110167.
(42) Kim, S. J.; Hasanyan, J.; Gemmell, B. J.; Lee, S.; Jung, S. Dynamic criteria of plankton jumping out of water. *J. R Soc. Interface* **2015**, *12*, 20150582.
(43) Lee, D. G.; Kim, H. Y. Impact of a superhydrophobic sphere onto water. *Langmuir* **2008**, *24*, 142−145.
(44) Gao, N.; Geyer, F.; Pilat, D. W.; Wooh, S.; Vollmer, D.; Butt, H.-J.; Berger, R. How drops start sliding over solid surfaces. *Nat. Phys.* **2017**, *14*, 191−196.
(45) Chen, H.; Liu, H.; Lu, X.; Ding, H. Entrapping an impacting particle at a liquid−gas interface. *J. Fluid Mech.* **2018**, *841*, 1073−1084.
(46) De Jong, E.; Wang, Y.; Den Toonder, J. M. J.; Onck, P. R. Climbing droplets driven by mechanowetting on transverse waves. *Sci. Adv.* **2019**, *5*, eaaw0914.
(47) Latikka, M.; Backholm, M.; Baidya, A.; Ballesio, A.; Serve, A.; Beaune, G.; Timonen, J. V. I.; Pradeep, T.; Ras, R. H. A. Ferrofluid Microdroplet Splitting for Population-Based Microfluidics and Interfacial Tensiometry. *Adv. Sci.* **2020**, *7*, 2000359.
(48) Nguyen, N. T. Deformation of ferrofluid marbles in the presence of a permanent magnet. *Langmuir* **2013**, *29*, 13982−13989.

https://doi.org/10.1021/acs.nanolett.2c00100
Nano Lett. 2022, 22, 2923−2933

(49) He, X.; Ni, M.; Wu, J.; Xuan, S.; Gong, X. Hard-magnetic liquid metal droplets with excellent magnetic field dependent mobility and elasticity. *J. Mater. Sci. Technol.* **2021**, *92*, 60−68.
(50) Wang, H.; Chen, S.; Li, H.; Chen, X.; Cheng, J.; Shao, Y.; Zhang, C.; Zhang, J.; Fan, L.; Chang, H.; Guo, R.; Wang, X.; Li, N.; Hu, L.; Wei, Y.; Liu, J. A Liquid Gripper Based on Phase Transitional Metallic Ferrofluid. *Adv. Funct. Mater.* **2021**, *31*, 2100274.
(51) Chechetka, S. A.; Yu, Y.; Zhen, X.; Pramanik, M.; Pu, K.; Miyako, E. Light-driven liquid metal nanotransformers for biomedical theranostics. *Nat. Commun.* **2017**, *8*, 15432.
(52) Liu, Q.; Fang, J.; Han, B. Novel electromagnetic repeated launch locking/unlocking device (RLLUD) based on self-locking for magnetic bearing flywheel. *Sens. Actuators, A* **2012**, *175*, 116−126.
(53) Timonen, J. V. I.; Latikka, M.; Leibler, L.; Ras, R. H. A.; Ikkala, O. Switchable Static and Dynamic Self-Assembly of Magnetic Droplets on Superhydrophobic Surfaces. *Science* **2013**, *341*, 253−257.
(54) Li, X.; Li, S.; Lu, Y.; Liu, M.; Li, F.; Yang, H.; Tang, S. Y.; Zhang, S.; Li, W.; Sun, L. Programmable Digital Liquid Metal Droplets in Reconfigurable Magnetic Fields. *ACS Appl. Mater. Interfaces* **2020**, *12*, 37670−37679.
(55) Fan, X.; Dong, X.; Karacakol, A. C.; Xie, H.; Sitti, M. Reconfigurable multifunctional ferrofluid droplet robots. *Proc. Natl. Acad. Sci. U. S. A.* **2020**, *117*, 27916−27926.
(56) Demirors, A. F.; Aykut, S.; Ganzeboom, S.; Meier, Y. A.; Poloni, E. Programmable droplet manipulation and wetting with soft magnetic carpets. *Proc. Natl. Acad. Sci. U. S. A.* **2021**, *118*, e2111291118.

https://doi.org/10.1021/acs.nanolett.2c00100
Nano Lett. 2022, 22, 2923−2933